Case Studies in Thermal Engineering 25 (2021) 100985

Contents lists available at ScienceDirect

Case Studies in Thermal Engineering

journal homepage: http://www.elsevier.com/locate/csite

Dual-separated cooling channel performance evaluation for high-power led Pcb in automotive headlight

Gökhan Sevilgen [a,*], Muhsin Kiliç [b], Mehmet Aktaş [c]

[a] Department of Automotive Engineering, Engineering Faculty, Bursa Uludağ University, Bursa, Turkey
[b] Department of Mechanical Engineering, Engineering Faculty, Bursa Uludağ University, Bursa, Turkey
[c] Magneti Marelli Mako Elektrik Sanayi Ve Tic. A.S., Bursa, Turkey

ARTICLE INFO

Keywords:
Automotive headlight
Liquid cooling
CFD
Thermal analysis
Junction temperature

ABSTRACT

In this paper, thermal and hydraulic analysis of a dual-separated cooling channel was performed for the cooling applications of different automotive lighting systems. A single LED and multi-LEDs were considered to evaluate the thermal and hydraulic performance as well as the lighting properties of automotive headlights. The detailed hydraulic analysis was theoretically evaluated for developing laminar flow to get higher thermal performance with less pumping power. The theoretical and simulation results for the dual-separated cooling channel were compared and discussed. Unlike the constant properties were used in the current literature, thermal analysis with temperature-dependent properties was performed to estimate Nusselt number preciously for dual-separated cooling channels. The temperature measurements were also performed in the experimental study to compare the numerical results. The light output parameter of the LEDs depends on junction temperature, it was found that the increase in light output by using a dual-separated cooling channel was about 10% for all cases. Otherwise, higher junction temperature values lead to a reduction in operating efficiency. The top copper surface temperature drop was higher than 50%, and the junction temperature had been reduced by 36% to ensure the desired operating conditions of the automotive lighting system.

1. Introduction

With the advances and developments in the manufacturing technology and materials, Light Emitting Diodes (LED) are becoming increasingly important parts of the automotive lighting applications [1]. Automotive industries we replacing the light source of their vehicle headlamps with LEDs in place of conventional Halogen and Xenon bulbs due to the advantages provided by LEDs, and these types of lighting systems began to compete with other lighting systems [2]. In addition, to supply the lighting functions, the main reason for preferring these elements include reasonable energy consumption, rapid response time, and long-lasting. One of the advantages of the LED technology headlights is their contribution to the driver and pedestrian safety because this new technology has more light output and brighter than halogen bulbs and these parameters aid driver visibility [3]. In the literature, driver visibility models were developed, which include headlamp type and efficiency parameters [4]. In this respect, the improved vehicle headlight can change accidents occurring at night [5]. With the development of LED technologies, matrix headlights had been developed to increase driving safety by illuminating the desired areas on the road. Instant illumination and high energy efficiency, LED technology

* Corresponding author.
E-mail address: gsevilgen@uludag.edu.tr (G. Sevilgen).

https://doi.org/10.1016/j.csite.2021.100985
Received 13 December 2020; Received in revised form 28 March 2021; Accepted 30 March 2021
Available online 14 April 2021
2214-157X/© 2021 The Author(s). Published by Elsevier Ltd. This is an open access article under the CC BY-NC-ND license (http://creativecommons.org/licenses/by-nc-nd/4.0/).

offered opportunities for smart automotive lighting systems.

On the other hand, more cooling capacity is needed due to the demand for higher lighting density and the occurrence of higher operating temperature values. In the LED systems, 65%–80% of the input power of a LED converts into heat while the rest of this is transformed into light. The produced heat is transferred through the connection junction of the LED to the printed circuit board (PCB). Meanwhile, this heat causes a dramatic rise in the junction temperature, which considerably decreases the thermal performance and lighting quality of the LED chipsets as well as shortens the expected operating life of LEDs. When the LED lighting switch on, the junction temperature of high-power LEDs rises quickly; thus, the junction temperature needs to be controlled; otherwise, overheating leads to a decrease in luminance as well as a reduction in operating efficiency [7,8]. Thus, the thermal management of high brightness multi-LED packages is still a challenge that can be improved [6]. The available thermal management of electronic systems can be classified into two main methods, known as i) passive cooling and ii) active cooling methods. The passive techniques include different applications such as using heat sinks, thermal interface material enhancements, improvements of components material considering thermal resistance, etc. [9]. During recent decades, engineers and experts had proposed a wide range of methods to improve the thermal performance of heat exchangers. However, the improved conventional cooling systems include metal heat sinks, and thermal interface material (TIM) was insufficient to meet the demands for thermal management of LED systems [10]. Active heat dissipation methods, like liquid cooling, presented better cooling performance. However, these systems had to be designed considering energy consumption and cost reduction. For instance, different cooling channels of thermal performance were evaluated by using different flow rates [11]. In another research proposed that different array of LEDs in a multi-led package system need different thermal management, and a staggering array was shown better thermal performance compared to the aligned ones [12]. The information about the thermal management of the LEDs make it easier to design an efficient and reliable LED system [13].

However, the cooling channel design was also observed in other applications such as microprocessors, power electronics cooling, LEDs, fuel cells, semiconductors, and transistors where they need to dissipate a high amount of heat from these elements. Liquid cooling channels can be classified by the hydraulic diameter of the channel. These cooling channels were known as conventional, minichannels, microchannels, and nanochannels in general. All these channels had different thermal performances and had been developing to reach more effective and innovative cooling methods [14]. The thermal and hydraulic performances of water cooling blocks were compared both numerically and experimentally for microelectronics cooling [39]. Moreover, detailed analytical techniques were also presented and discussed [15]. Single-phase liquid cooling in different multi-microchannel heat sink configurations was studied experimentally and numerically to get the effects of flow separation and redirection on the microchannel heat sink of electronic systems [16,17]. An analytical and experimental method was proposed to understand the heat transfer and pressure drop in serpentine channel heat sinks by using the thermal resistance network method. A CFD model was used to get the bending loss in pressure drop calculations of the serpentine channel for electronic cooling [18]. The experimental investigation on heat transfer and hydrodynamic characteristics of nanofluid as a coolant in wavy channel heat sinks had three different channel configurations was studied [38]. An experimental investigation on the pressure drop and frictional behavior of air flow through helical micro-tubes with circle, triangle, square and pentagon geometries with different coil diameter was performed and the effect of flow rate, coil diameter and geometry were examined on the pressure drop and friction factor [41]. Another application about the improvement of thermal performance of heat exchangers was using vortex generators that augment the thermal efficiency of heat exchangers by creating vortices, swirl flows and subsequent breaking of thermal boundary layer [42]. Among the all these methods, the passive methods are those type of mechanisms at which no external forces are used. On the other side, the active methods are those in which the external force is the agent of the heat transfer enhancement factor. Amongst various active heat transfer methods, the air injection or more generally, the use of gas–liquid two-phase flow has gained significant attention [43]. Many of these researches in the available literature described above were based on the thermal performance of liquid cooling channels related to the electronics cooling applications in general, but there was a few research based on the liquid cooling of automotive lighting systems in the available literature. Thus, this paper could be used as a reference study in further investigations for the design of cooling blocks used for the purpose of automotive LED lighting systems [35,36].

In this paper, both thermal and hydraulic performance of a liquid cooling system designed for high power LED of the automotive lighting system was performed. Besides thermal and hydraulic performance, lighting properties and operating conditions also had a great effect on the lighting systems. Thus, lighting characteristics that depend on temperature were also presented and discussed. Thermal performance was achieved by using three-dimensional CFD simulation, and also an experimental study of a standard high power LED was performed for getting reference data to compare the numerical results. The hydraulic performance was theoretically evaluated by developing laminar flow to get higher thermal performance with less pumping power. In industrial applications, these improvements in heat transfer rates were achieved for higher pressure drops. In contrast, this study was aimed to provide this desired thermal performance by using lower mass flow rates. Although there were several studies in the literature regarding the liquid cooling channels related to the electronics cooling applications in general, there were a few research based on the liquid cooling of automotive lighting systems include single or multi-LED applications. It seemed that this physical phenomenon related to LED applications in automotive lighting systems had not been considered in the published studies.

The aim of this paper is to present a new design method for liquid cooling applications of automotive lighting systems to provide operating conditions that LED lighting system runs without damage. Another objective of this work is to provide the required performance of such liquid cooling systems by means of detailed hydraulic and thermal analyses considered together.

With the consideration given above, the novelty of the present research and the main contributions to the scientific literature of this research can be stated as follows; a novel LED cooling block with dual-separated liquid cooling channel was designed and manufactured for the automotive lighting system with using different heating powers about single and multi-LEDs applications. A detailed hydraulic analysis was described for evaluating the developing laminar flow in the cooling block. The more realistic three dimensional

CFD model included temperature-dependent properties was realized to get the fluid flow and conjugate heat transfer analysis of dual-separated cooling channel. Generalized Nusselt number correlations were obtained with temperature-dependent properties for such separated cooling channels. It was shown that lighting characteristics of automobile head lamps can be improved by using such separated cooling channels. An experimental study was also conducted by using manufactured real LED PCBs and the dual-separated liquid cooling block designed for the automotive lighting system.

The paper was organized as follows: Dual-separated liquid cooling channel designed and manufactured for the automotive lighting system was described in section 2.1. A detailed hydraulic analysis was presented in section 2.2 for evaluating the developing laminar flow in the liquid cooling block. The three-dimensional CFD model included temperature-dependent properties and conjugate heat transfer analysis of dual-separated cooling channel were described in section 2.3. An experimental study and the list of measurement devices used in the experiments were described in section 2.4. The validation of the numerical results was presented in section 2.5. The results of this study were presented and discussed in section 3, and finally, the main conclusions were evaluated in section 4.

2. Material and methods

2.1. LED system with dual-separated cooling channel

In this study, a single LED on the printed circuit board of an automotive headlight system was designed and manufactured by using advanced technologies, and the selected LED was composed of LED case, lead frame, encapsulate, source, chip, and the layer parts. The LED case was a plastic housing that protected the LED, and the Lead frame provided electrical transmission between the LED chip and solder; encapsulate was a plastic-based filler material that filled the interior volume of the LED. Source, Chip, Layer, were the light produced parts from LED.

The LED PCB employed in this work consist of two different zones. The first zone included the TIM layer between the top and bottom copper plates, cover layer (or heat sink), and the installation of the liquid cooling block on the automobile headlight developed in this study are shown in Fig. 1a, b, and 1c, respectively. The second zone was a liquid cooling block in which dual-separated liquid flow channels placed, demonstrated in Fig. 2a and Fig. 2b. After entering in the cooling block, the water flow separated into two parallel flow regions so that to obtain a homogenous temperature distribution on the cover or heat sink plate. The sectional view (A-A) of the whole single LED system and the dimensions of the cooling block are shown in Fig. 2c and d, respectively. The sizes of the cooling block were small enough that the length and the width of the whole cooling block were 73 mm and 64 mm, respectively. The height (H_c) and the width (W_c) of the cooling channel were designed as 9 mm and 5 mm, respectively, so that the aspect ratio of the channel

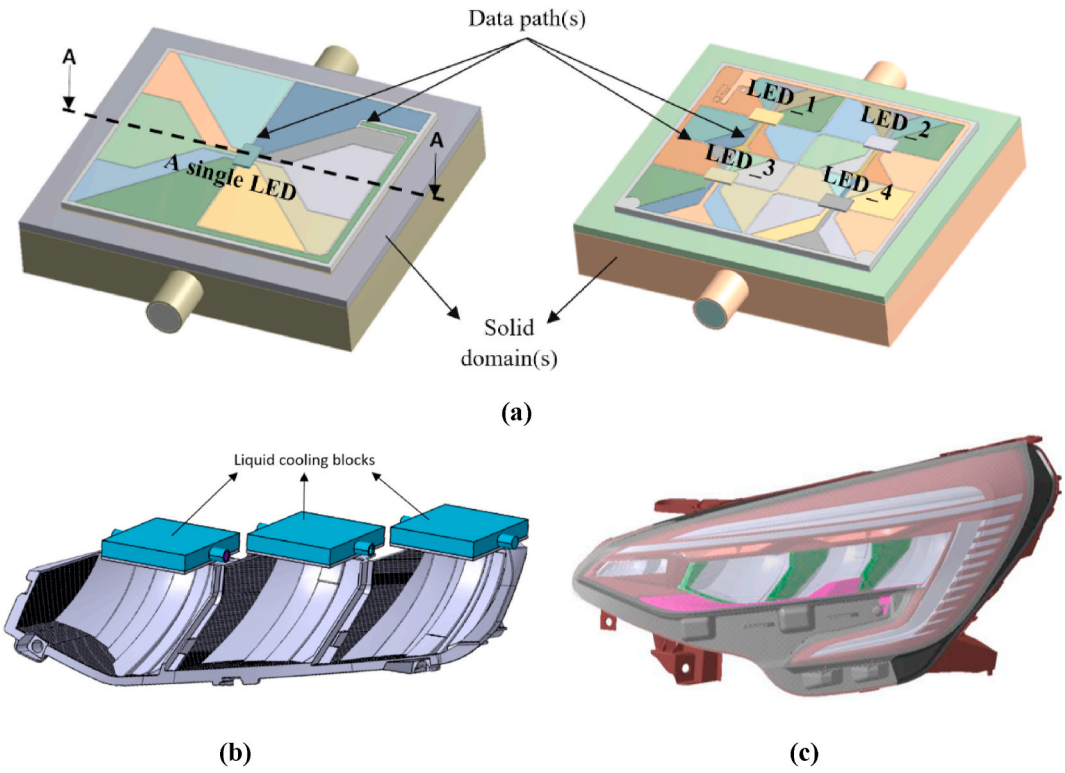


Fig. 1. (a) The sectional view and the subcomponents of the high power LED used in this study The proposed lighting system include (b) a single and multi-LED, (c) the installation of the cooling block on the reflector and (d) automobile head lamp used in this study.

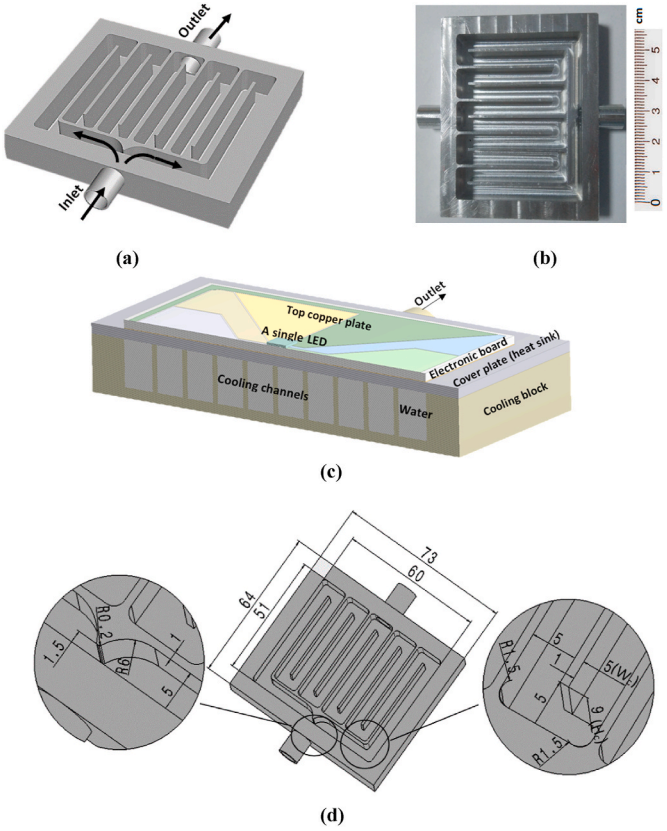


Fig. 2. The dual-separated cooling channel (a) CAD model, (b) the manufactured prototype (c) the cross-sectional view (section A-A) of a single LED system, (d) the dimensions (mm) of the designed dual-separated cooling channel.

was about 0.6 and hydraulic diameter was calculated about 6 mm.

2.2. Theoretical calculations

2.2.1. Flow and pressure drop analysis

The total pressure drop can be calculated considering minor and major losses that occurred in the liquid cooling channel used in this study. The minor losses had three components for this channel. The first and the third components were happened due to sudden contraction (ΔP_c) or extraction (ΔP_e) at the fluid inlet and outlet regions of the cooling channel, respectively. The second component was occurred at the entrance region and also in the cooling channel due to 90° bending losses ($\Delta P_{bj,90^\circ}$). The major pressure losses occurred due to friction (ΔP_f) and 180° returns ($\Delta P_{bi,180^\circ}$) in the cooling channel. Due to flow separation into two parallel flow regions, the total pressure drop can be calculated for half part of the cooling channel, and the locations of these pressure drops are demonstrated in Fig. 3c.

The channels in the cooling block were rectangular with a constant cross-sectional area. The flow in the channels was assumed as laminar. With this respect, the laminar flow hydrodynamic entrance length (L_h) can be calculated by means of Equation (1) [19].

$$L_h \approx 0.05\, Re\, D_h \tag{1}$$

where Re and D_h represent Reynolds number and hydraulic diameter, respectively. Reynolds number and hydraulic diameter can be defined as given in Equations (2)–(5), respectively.

$$Re = \frac{\rho_f\, U_{ch}\, D_h}{\mu_f} \tag{2}$$

$$T_{avg} = \frac{T_{in} + T_{out}}{2} \tag{3}$$

$$U_{ch} = \frac{\dot{m}}{\rho_f A_{ch}} \tag{4}$$

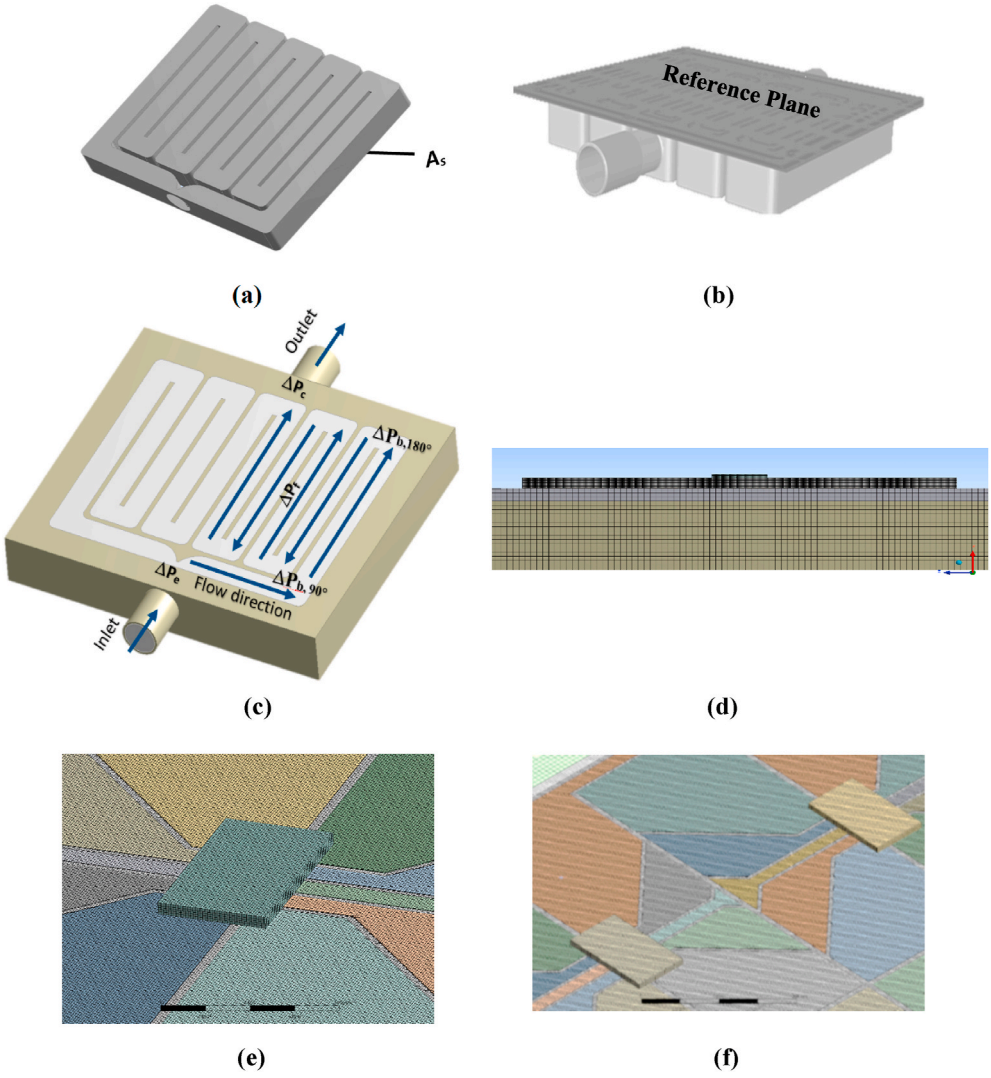


Fig. 3. a) The total surface area subject to the convective heat transfer (A_s), (b) the surface of the reference plane, (c) Computational fluid domain for all LED systems and the locations of pressure drop components demonstrated in a single flow region of the dual-separated cooling channel, (d) the sectional view of mesh structure; (e) the surface mesh of the LED system with using a single LED and (f) with using multi-LED.

$$D_h = \frac{2(W_c.H_c)}{(W_c + H_c)} \tag{5}$$

The density (ρ_f) and the dynamic viscosity (μ_f)of the fluid can be obtained at the average temperature (T_{avg}) of the inlet (T_{in}) and outlet (T_{out}) (Equation (3)). By using the temperature-dependent functions defined in section 2.3, thermal properties were taken at this average temperature of the fluid described in Eq. (3) and all theoretical calculations described in pressure drop and heat transfer analysis were performed considering this average temperature. Mass flow rate ($\dot{m}$)and the cross-sectional area (A_{ch}) of the channel can be used to obtain the average flow velocity (U_{ch}), as shown in Equation (4). The hydraulic diameter (D_h) of the channel can be calculated by using the width (W_c) and the height (H_c) of the channel as given in Equation (5).

The pressure drop was commonly obtained by using the fanning friction factor. Since the developing flow occurred through the entrance region, the total pressure drop resulted from friction in the channel included the contributions of both developing and fully developed flow zones. On the other hand, the apparent friction factor (f_{app}) for circular and noncircular channels can be used, including developing flow effects, and it can be calculated through Equation (6) correlated for single-phase flow. L and L^+ in Equation (7) represents the dimensional and the non-dimensional lengths of the channel, respectively. $K(\infty)$ denotes the incremental pressure drop in the fully developed region. c represents the fitting factor. Both of $K(\infty)$ and c were defined as the functions of the aspect ratio (α) as given in Equations (8) and (9), respectively. Meanwhile, aspect ratio (α) given in Equation (10) is the ratio of the smaller length (W_c) to the greater length (H_c) of the channel cross-section [20,21].

$$f_{app} = \frac{3.44}{Re\sqrt{L^+}} + \frac{\left(f_{fd} \cdot Re\right)_{fd} + \frac{K(\infty)}{4L^+} - \frac{3.44}{\sqrt{L^+}}}{Re\left(1 + \frac{C}{(L^+)^2}\right)} \tag{6}$$

$$L^+ = \frac{L/D_h}{Re} \tag{7}$$

$$K(\infty) = 0.674 + 1.2501\alpha + 0.3417\alpha^2 - 0.8358\alpha^3 \tag{8}$$

$$c = \left(0.1811 + 4.3488\alpha + 1.6027\alpha^2\right) \times 10^{-4} \tag{9}$$

$$\alpha = \frac{W_c}{H_c} \tag{10}$$

In Equation (6), the fanning friction factor (f_{fd}) can be obtained with the function of aspect ratio as given in Equation (11) [19].

$$f_{fd} = \frac{24}{Re}\left(1 - 1.3553\alpha + 1.9467\alpha^2 - 1.7012\alpha^3 + 0.9567\alpha^4 - 0.2537\alpha^5\right) \tag{11}$$

The total pressure drop because of the friction in the rectangular channel can be obtained by means of Equation (12) It should be noted that the channel length, L (m), is the summation of all straight and curved lengths.

$$\Delta P_f = \frac{\rho_f \cdot U_{ch}^2}{2}\left(\frac{4f_{app}\,L}{D_h}\right) \tag{12}$$

One of the major pressure drops appeared when the flow was reversed by 180°. This can be obtained by means of Equation (13) [22]. The quantity of reversing in the channel was considered with n in Equation (13), and the bending loss coefficient, ξ, can be obtained by the functions given in Equations (14) and (15), for respective Reynolds number. The curvature ratio, C_r, was defined by the ratio of the curvature radius to the channel hydraulic diameter; β was the ratio of the channel height to its width.

$$\Delta P_{b,180^\circ} = \frac{1}{2}\rho_f \cdot U_{ch}^2 \sum_{i=1}^{n} \xi_i \tag{13}$$

for 100< Re < 1000 (14)

$$\xi = 0.46(Re)^{1/3}\left(1 - 0.18C_r + 0.016{C_r}^2\right) \times \left(1 - 0.2\beta - 0.0022\beta^2\right)\left(1 + 0.26\left(\frac{W_t}{D_h}\right)^{2/3} - 0.0018\left(\frac{W_t}{D_h}\right)^2\right) \tag{14}$$

for 1000 < Re < 2200 (15)

$$\xi = 3.8\left(1 - 0.22C_r + 0.022{C_r}^2\right) \times \left(1 - 0.1\beta - 0.0063\beta^2\right) \times \left(1 + 0.12\left(\frac{W_t}{D_h}\right)^{2/3} - 0.0002\left(\frac{W_t}{D_h}\right)^2\right) \tag{15}$$

On the other hand, sudden extraction or contraction of the flow in the channel results in the minor pressure losses. These can be obtained by means of Equation (16), where K_e and K_c represent the extraction or contraction loss coefficients, respectively. They were calculated through Equations (17) and (18), respectively [15,23].

$$\Delta P_{e(or\ c)} = K_{e,}(or\ K_c)\ \frac{1}{2}\rho {U_{ch}}^2 \tag{16}$$

$$K_e = \left(1 - \frac{A_{out,}}{A_{in}}\right)^2 \tag{17}$$

$$K_c = 0.42\left(1 - \frac{A_{out}}{A_{in}}\right) \tag{18}$$

where A_{in} and A_{out} represent the inlet and outlet areas, respectively, of the contraction or extraction sections. The minor pressure losses occurred resulted in 90° bending at the entrance region of the channel. It could be obtained utilizing Equation (19), where was the bending loss coefficient, $K_{b,j}$, taken as a constant value of 1.2 [24].

$$\Delta P_{bj,90^\circ} = K_{b,j}\frac{1}{2}\rho {U_{ch}}^2 \tag{19}$$

The total pressure drop can be rewritten, as stated in Equations (20) and (21) by using Equations (12), (13), (16) and (19).

$$\Delta P_{total} = \Delta P_f + \Delta P_{bj,90^\circ} + \Delta P_{bi,180^\circ} + \Delta P_e + \Delta P_c \tag{20}$$

$$\Delta P_{total} = \frac{\rho_f \cdot U_{ch}^2}{2}\left(\frac{4f_{app}\,L}{D_h} + \sum_{i=1}^{n}\xi_i + \mathrm{K}_c + \mathrm{K}_e + \mathrm{K}_{b,j}\right) \tag{21}$$

In the theoretical calculations, the mass flow rate of water was ranged from 0.0001 kg/s to 0.025 kg/s, and these values were selected as considering the laminar flow regime due to get higher thermal performance with less pumping power. Several cases were considered to compare the data in this research work, and the mass flow rates varied between 0.00025 and 0.005 kg/s.

2.2.2. Heat transfer analysis

Steady-state heat transfer rate to the cooling fluid from the LED PCB was calculated utilizing the energy balance as given Equation (22), where, $\dot{Q}_b$ was the released total heat transfer rate transferred to the flowing coolant in the block, $\dot{m}$ represents the total mass flow rate of the coolant, T_{in} and T_{out} were the fluid temperature at the inlet and outlet of the cooling block, respectively. V and I indicate the voltage and current provided by the power supply to a single LED, and the q_{loss} was the required heat loss rate for the lighting function of a single LED used in this study.

$$\dot{Q}_b = \dot{m}\, c_p\, (T_{out} - T_{in}) = I.V - q_{loss} \tag{22}$$

The convection heat transfer rate between the channel surfaces and the coolant fluid was formulated by employing LMTD approach as given in Equation (23), where h_{avg} represents the averaged convective heat transfer coefficient. A_s denotes the total area of wetted surfaces subject to the convective heat transfer as shown in Fig. 3a. The value of ΔT_{lm} can be obtained using Equations (24) and (25). Since the block surface temperature was not homogenous, a reference plane (Fig. 3b) in the solid zone was employed, which was adjacent to the fluid volume, and the average of the reference solid surface temperatures was engaged in the calculation of LMTD.

$$\dot{Q}_b = h_{avg.}\, A_s\, \Delta T_{lm} \tag{23}$$

$$\Delta T_m = \frac{\Delta T_1 - \Delta T_2}{\ln(\Delta T_1/\Delta T_2)} \tag{24}$$

$$\Delta T_1 = T_{ref} - T_{in}\ ,\ \Delta T_2 = T_{ref} - T_{out} \tag{25}$$

By using Equations (22) and (23), the average heat transfer coefficient can be obtained. Then, Nusselt number as defined in Equation (26) was calculated by employing the fluid thermal conductivity, k_f, and the hydraulic diameter of the channel, D_h, and the average heat transfer coefficient. On the other hand, the average Nusselt number (Nu_{fd}) for the fully developed regime can be calculated by using Equation (27).

$$Nu = \frac{h_{avg.} D_h}{k_f} \tag{26}$$

$$Nu_{fd} = 8.235\left(1 - 1.883\propto + 3.767\propto^2 - 5.814\propto^3 + 5.361\propto^4 - 2\propto^6\right) \tag{27}$$

The junction temperature, T_j was calculated by using Eq. (28).

$$T_j = T_{max} + P_{LED} R_{th,Jp} \tag{28}$$

where T_{max} represents the obtained highest temperature on the copper plate top surface of the LED PCB; $R_{th,jp}$ denotes the real thermal resistance of the junction point; P_{LED} gives the LED power.

2.3. Numerical simulations

The combined model of the solid and fluid volumes is given in Figure- 3c. The finite volume numerical method was employed to perform the computation to solve the flow field and to obtain conjugate heat transfer in both solid and fluid regions. Numerical computations to solve governing equations as conservation, transport, and energy equations were realized by using Ansys Fluent. Detailed information and descriptions of the numerical methods can be found in Refs. [25,40].

The numerical model includes all heat transfer modes, and the continuity, momentum, and energy equations for steady-state conditions of water flow with variable properties can be written by using Equations (29)–(31), where $\vec{V}$ (m/s) is the velocity vector; p (Pa) is the pressure; μ(Pa.s) is the fluid dynamic viscosity; T (°C) is the temperature; ρ (kg/m^3) is the density of fluid in the computational domain.

The continuity equation for the fluid domain may be given as follow.

$$\nabla\left(\rho\vec{V}\right) = 0 \tag{29}$$

Momentum conservation equations in x, y, and z directions, respectively, are given as follows.

$$\vec{V}.\nabla\left(\rho\vec{V}\right) = -\nabla p + \nabla.\left(\mu\nabla\vec{V}\right) \tag{30}$$

The energy equation for the fluid domain can be written by using Equation (31) for the fluid zone with steady-state conditions, where, $\vec{V}$(m/s) is the velocity vector; c_p (J/kgK) is the fluid specific heat; k_f (W/mK) is the fluid thermal conductivity. For solid zones, the energy equation can be written in Equation (32), where S denotes a source term such as heat generation in the LED volume, and the source term can be ignored in the other region of the solid volumes, and k_s (W/mK) gives the thermal conductivity of solid material [33].

$$\vec{V}.\nabla\left(\rho c_p T\right) = \nabla.\left(k_f \nabla \mathrm{T}\right) \tag{31}$$

$$\frac{\partial}{\partial x}\left(k_s \frac{\partial T}{dx}\right) + \frac{\partial}{\partial y}\left(k_s \frac{\partial T}{dy}\right) + \frac{\partial}{\partial z}\left(k_s \frac{\partial T}{dz}\right) + \mathrm{S} = 0 \tag{32}$$

In the computations, the average temperature value of the fluid (Equation (3)) was employed to determine the fluid properties such as specific heat (c_p), thermal conductivity (k_f), density (ρ), dynamic viscosity (μ) and also Prandtl number (Pr). The increase or decrease in temperature affects the fluid properties, and these effects can be used in the CFD calculations by using temperature-dependent properties. For this purpose, the temperature-dependent functions were defined for these properties except fluid density (kg/m^3) because the change in fluid density versus temperature variations was negligible for the operating conditions used in this study. The calculated temperature-dependent thermal properties for the temperature of the fluid between 285 K and 315 K by using Equations (33)–(35) and the comparison to the reference data is shown in Table-1.

$$k_f(T) = 0.0015\ T + 0.1621 \tag{33}$$

$$c_p(T) = 0.0176\ T^2 - 10.912\ T + 5869.36 \tag{34}$$

$$\mu\ (T) = 0.0069 - 0.00002\ T \tag{35}$$

It is well known that mesh structure is very crucial for the accuracy of the computed results and the computation time [26–29]. Therefore, a hexahedral mesh structure was employed in the Cartesian coordinate system. Considering the high-temperature gradients around the LED chip, high mesh intensity with a size of about 10 mm × 15 mm exists in that region. The computational domain consisted of about four million elements in total. Fig. 3d, e and f shows the some parts of the mesh structure used in the computations. The boundary conditions applied in the numerical model are given in Table 2.

In the numerical simulation, SIMPLE algorithm was employed for the coupling of pressure-velocity, and the calculations were conducted for the steady-state conditions. The normalized residuals of the governing equations were considered for the convergence criteria. During the computations, it was accepted that the numerical simulation was converged when the normalized residuals of the continuity and momentum equations were less than 10^{-6} and the energy equation was less than 10^{-8}. No-slip boundary condition was used for solid-fluid boundary surfaces, and the ambient air temperature was assumed as a constant value of 23.45 °C considering experimental conditions. The power of LED was taken as a value of 3 W, and this was simulated by volumetric heat generation in the LED chip volume. For the outer walls of the cooling block surrounded by air, mixed boundary conditions were applied to consider the heat transfer effects of the radiation and the free convection. The thickness of the copper plates placed at the bottom and top sides of PCB was 35 μm and LED printed circuit board material was chosen as FR4. In computations, at the fluid inlet area of the cooling block, different coolant mass flow rate values between 0.0002 and 0.005 kg/s were considered to achieve better thermal efficiency with lower total pressure losses. According to the experimental work, the constant value of 23.45 °C was taken as the coolant inlet temperature.

2.4. Experimental set-up

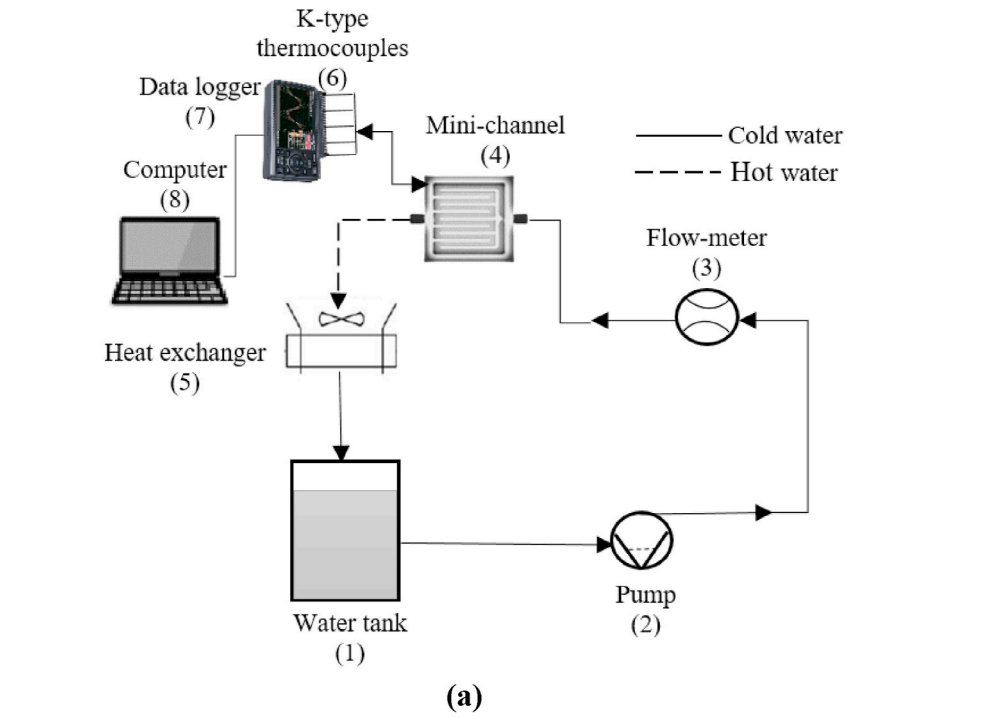
The schematic view of the experimental set-up for a single LED system is shown in Fig. 4a. The components of the test rig were (1) a cooling fluid tank, (2) a pump, (3) a turbine-type volumetric flow meter, (4) dual-separated flow channel, (5) the heat sink unit, (6) several K-type thermocouples, (7) a data logger and (8) a computer. The pump consumed a reasonable power to recirculate coolant, and the maximum flow rate of this pump ($\dot{V}_p$) was 8 l/min and it provided an upper limit of the temperature value of 90 °C. The operating flow rate of the flow meter measuring device was changed between 0 and 30 l/min and the operating temperature was in the range of −20 °C–120 °C. This type of flow meter device was designed especially for lower mass flow rates of liquid coolants. For

Table 1
Variable propertied of fluid used in the numerical calculations and comparisons to the reference data [34].

T (K)	Reference Data	Calculated	Reference Data	Calculated	Reference Data	Calculated
	k_f (W/mK)	k_f (W/mK)	c_p (J/kgK)	c_p (J/kgK)	μ. (Ns/m^2)	μ. (Ns/m^2)
285	0.590	0.590	4189	4189	0.00123	0.00120
290	0.598	0.597	4184	4185	0.00108	0.00110
295	0.606	0.605	4181	4182	0.00096	0.00100
300	0.613	0.612	4179	4180	0.00086	0.00090
305	0.620	0.620	4178	4178	0.00077	0.00080
310	0.628	0.627	4178	4178	0.00070	0.00070
315	0.634	0.635	4179	4178	0.00063	0.00060

Table 2
Boundary conditions applied in the computations.

Area or Volume	Conditions
Coolant fluid inlet area	Mass flow inlet with a temperature of 23.45 °C
Coolant fluid outlet area	Pressure exit conditions (0 Pa)
Coolant mass flow rate	Range from 0.0002 kg/s to 0.005 kg/s
Single or multi-LEDs chip	Heat generation rate depends on operating conditions
Outer walls	Mixed boundary condition (Free convection and radiation)
Solid walls	$\vec{V} = 0$
Solid Volume	**Material**
Dual-separated cooling block	Aluminum
LED chip	Chip material
Cover plate of the cooling block	Aluminum
Copper plates	Copper
Thermal Interface Layer	TIM (Thermal insulation material)
PCB	FR4 (Glass-reinforced-epoxy laminate)



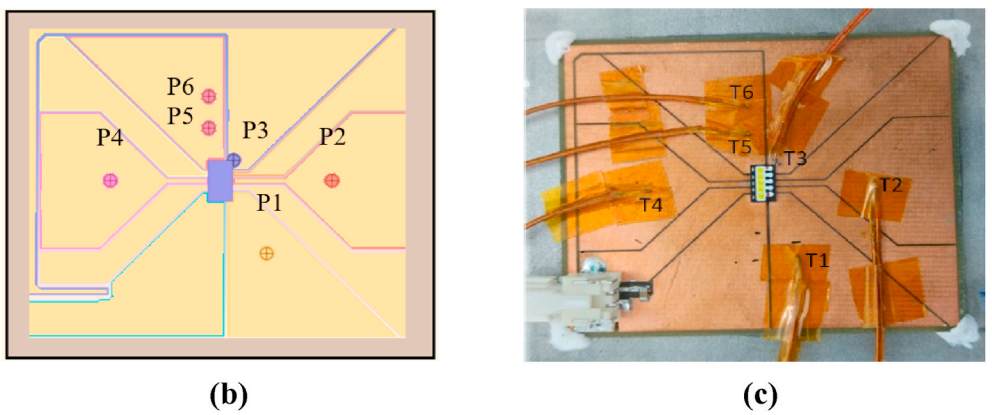


Fig. 4. (a) The schematic view of the experimental set-up (b) the locations of the data points: (b) simulated PCB in the numerical model; (c) PCB used in the experimental work.

providing the constant temperature value of the coolant entered in the cooling channel, a compact heat exchanger unit was added to the system. The power unit was used to control the current value of LED chip, and the flow rates were observed instantly by integrating the measurement device into this unit. The fluid can flow between the components of the test rig via flexible PVC pipes.

For getting comparative results between experimental and numerical data, the temperature measurement points were defined on the top copper surfaces shown in Fig. 4b and c. This temperature data was used to evaluate the cooling performance of the dual-separated cooling channel, and these measurements were performed for LED system. For this purpose, different temperature measurement locations were determined from P1 to P6 on the top copper surfaces. The experimental apparatus employed for the measurements of flow rate and temperature are given in Table 3. Temperature data was measured with K-type thermocouples, and the flow rate was measured with a turbine-type volumetric flow meter. In order to find out the total experimental error, an uncertainty analysis was performed according to the method proposed by Moffat [30]. The highest uncertainty in experimental data was calculated to be within ± 3%.

2.5. Validation of the numerical results and mesh independent analysis

- The comparison between numerical results and theoretical calculations of the total pressure drop in dual-separated cooling channel depends on the mass flow rate is shown in Fig. 5a. The total pressure drop significantly increased with increasing mass flow rate. It was about 11 Pa for the mass flow rate of 0.002 kg/s. The highest value was obtained about 50 Pa for the case of 0.005 kg/s which was the maximum flow rate considered in this work. From the comparison of the total pressure drop, we can easily say that the predicted total pressure drop numerically had the same trend with the theoretical data, and the maximum deviation was lower than 10% in general. From these results, we can say that the numerical results had good agreement with the theoretical data obtained by using Equation (21) from this study. The mesh independent analysis was also performed of a single LED system and it was found that about four million elements in total were enough for the mesh-independent analysis and the results for the case of 0.002 kg/s were shown in Figure- 5c.

The calculated temperature values obtained from the numerical study at different locations (from P1 to P6) of the top copper plate surface of a single LED system are shown in Table 4. Predicted temperature values on the top copper surface of a single LED system for the case of 0.002 kg/s mass flow rate and the comparison with the experimental data are also presented in Fig. 5b. These temperature measurements were used as reference data for the cooling performance, and the experiments were only considered for a single LED lighting system. The temperature difference between experimental data and numerical results obtained for the case of 0.002 kg/s was lower than 3 °C in general; thus, we can easily say that the temperature predictions for top copper surface were in good agreement with the experimental data obtained from this study.

From these numerical results, higher temperature values predicted close to the LED for P3 location due to higher heat generation rate. The temperature value for P3 location obtained from the experimental study was about 85 °C without using this cooling channel, and this value was decreased to 45 °C for the case of 0.002 kg/s which had lower mass flow rate. The decrease in temperature was about 50% in percentage for P3 location. For the other locations, this value was calculated about 60% in percentage, where the locations far away from LED on the top copper surface. The predicted maximum temperature was ranged from 66.5 °C to 68.8 °C for all cases, and by using Equation (28), the junction temperature was calculated between 69 °C and 71 °C, which was lower than the upper limit of the junction temperature of 150 °C so that a single LED operated without damage. From the numerical and experimental results of temperature distributions by using this dual-separated cooling channel, the decrease in temperature was higher than 50% on the top copper surface contact with LED chip, and the junction temperature had been reduced by 36% to ensure desired operating conditions compared to the without cooling.

3. Results and discussion

The calculated velocity values for the case of 0.001 kg/s, which had a moderate mass flow rate is shown in Fig. 6a. The maximum estimated velocity value was about 0.045 m/s for this case, and the calculated average velocity in the cooling channel was about 0.010 m/s. From these results, the recirculating flow regions were observed near the bending and flow separation areas depends on the higher velocity values that occurred in the cooling channel, which tended to an increase in convective heat transfer. The calculated temperature values on the middle section of the dual-separated cooling channel for a single LED and multi-LED systems are shown in Figures, 6b and 6c, respectively. The temperature difference between inlet and outlet sections was calculated about 1 °C for a single LED system, whereas this value was calculated about 4 °C for a multi-LED system at the same mass flow rate (0.001 kg/s).

From the results of the predicted temperature values on the middle plane of the dual-separated cooling channel for a single LED system, the increase in temperature of the water was calculated about 1.5 °C for the case of 0.0005 kg/s and this value was calculated

Table 3
The measurement apparatuses accommodated in the experimental work.

Kind	Measuring range	Accuracy
Temperature measurement K-type thermocouple	−40 °C/400 °C	±0.75%
Mass flow rate measurement of flowmeter	0–30 l/min	±1%

Table 4
The calculated temperature (°C) values obtained from the numerical study at different locations defined on the top copper surface of a single LED system with lower mass flow rates.

Temp. measurement points	0.00025 kg/s	0.00050 kg/s	0.00100 kg/s	0.00200 kg/s	0.00400 kg/s	0.00500 kg/s	Measured Temperature (°C) values (Without cooling)
P1	30.25	29.08	28.49	28.19	28.02	27.98	68.00
P2	26.20	25.10	24.49	24.20	24.05	24.01	62.00
P3	44.97	44.41	44.13	43.99	43.89	43.86	85.00
P4	26.30	25.15	24.58	24.29	24.13	24.11	65.00
P5	38.68	37.54	36.97	36.68	36.52	36.49	80.00
P6	30.76	29.63	29.07	28.79	28.64	28.61	71.00
T_{max}	68.75	67.58	66.99	66.69	66.52	66.49	–
T_j	70.92	69.75	69.16	68.86	68.69	68.66	110.50

about 0.2 °C for the case of 0.004 kg/s' which had higher mass flow rate. Another significant result was that for the case of 0.0005 kg/s, the middle plane had a more homogeneous temperature distribution for all considered cases. Meanwhile, the calculated temperature distribution on the middle plane of the dual-separated cooling channel for the multi-LED system is shown in Fig. 6d and e, and the calculated temperature results varied from 23.45 °C to 30 °C for the multi-LED system. The increase in temperature of the water was predicted at about 6 °C for the case of 0.0005 kg/s due to high heat transfer from the multi-LED system. This value was reduced to 1.0 °C depends on the water mass flow rate selected for the case of 0.004 kg/s.

The predicted temperature values of the top copper surfaces of a single LED system are shown in Fig. 7a and Fig. 7b. The higher temperature values were obtained close to the LED chip, and the maximum value was calculated at about 66 °C for the last case, which had the highest mass flow rate (0.004 kg/s). On the other hand, the calculated temperature values were rapidly decreased depends on the distance from LED, and this leads to higher temperature gradients near the LED chip, and lower temperature gradients were obtained far away from the LED chip. Another important result was that the data paths on the top copper surface had a great effect on the temperature distribution of the top copper surface because these paths served as a thermal bridge between the subcomponents of this surface. The predicted temperature values of the top copper surfaces of the multi-LED system are shown in Fig. 7c and d. The calculated maximum temperature value was about 75 °C for the case of 0.0005 kg/s mass flow rate, and this value was reduced to about 70 °C for the case of 0.004 kg/s mass flow rate. These values were predicted higher than the temperature values obtained from the numerical simulations of a single LED system, but these temperature values were also lower than the upper limit of the junction temperature of 150 °C so that LED operated without damage. As a result, we can easily say that the liquid cooling block designed for a single and multi-LED system fulfilled the need for the cooling of lighting system.

The Nusselt correlations for the calculating average Nusselt number for such liquid cooling blocks in the available literature were based on two kinds of boundary conditions such as constant heat flux [37] or constant temperature. However, a non-uniform temperature distribution occurred on the LED PCB cooled with the dual-separated cooling channel used in this study. Thus, the heat transfer characteristics between the LED PCB and the cooling block had unique properties, and the calculated average Nusselt number and the calculated average convective heat transfer coefficient are shown in Fig. 8a and Fig. 8b. The calculated average Nusselt number varied from 8.35 to 15.82 for a single LED system, and this value changed between 8.03 and 14.72 for the multi-LED system in general. However, the computed average Nusselt number for the cases which had higher mass flow rates computed about 16.0 and 15.0 for a single and multi-LED system, respectively. This means that the cases operating with lower mass flow rates provided a considerable increase in heat transfer compared to the cases with higher mass flow rates. The calculated average convective heat transfer coefficient is shown in Fig. 8b, and these values ranged from 789 W/m^{2}K to 1493 W/m^{2}K for a single LED system, and these values changed between 760 W/m^{2}K and 1390 W/m^{2}K for the multi-LED system.

From the numerical calculations, Nusselt number correlations obtained for the separated cooling channel used with a single and multi-LED system were proposed as follows. R^2 value of Equations (38) and (39) was 0.99, and the proposed correlations predicted *Nu* values for the dual-separated cooling channel with plane cover within ±5% difference ratio.

$$Nu = 0.81 Re^{0.397} Pr^{1/3} \tag{38}$$

$$Nu = 0.77 Re^{0.365} Pr^{1/3} \tag{39}$$

The calculated Nusselt numbers were compared to the experimental data, which was obtained for a straight rectangular channel used in Ref. [31]. The predicted Nusselt numbers were higher than the reference data because the cooling channel used in this study had separated flow regions, bends, and 180°returns, which aided in improving the convective heat transfer coefficient. On the other hand, the calculated average Nusselt number by using equation (27) for fully developed laminar flow was a constant value of 4.32; however, for developing laminar flow, the computed *Nu* number increased with Reynolds number. Considering all these parameters described above, the computed average Nusselt number from the results of the simulation showed very well agreement with the available experimental data in the current literature [31,32].

We conclude that in such liquid cooling blocks, approximate Nusselt correlation ($Nu_{approx.}$) can be rewritten from these results in a general form as follow. It can be said that constant C had a little change in terms of the total heat dissipation from LED lighting system, but this constant could be quite different when the cooling block type was different [33].

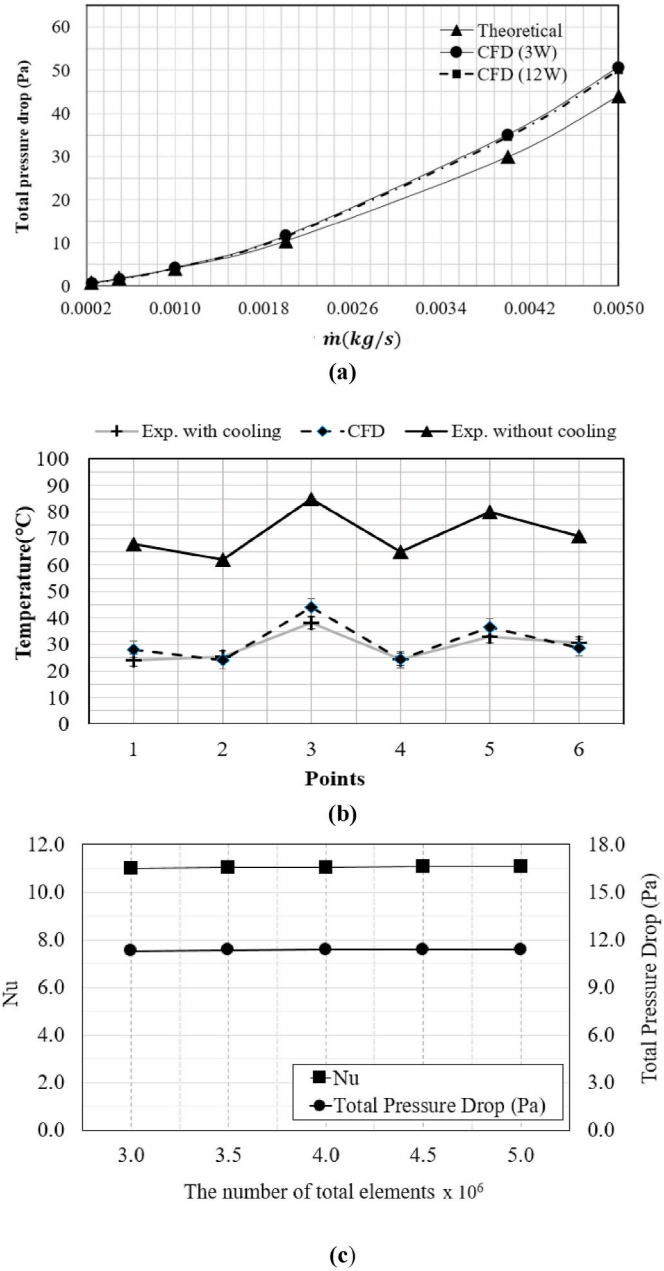


Fig. 5. (a) The comparison between numerical results and theoretical calculations of total pressure drop (ΔP_{total}) (b) and the predicted temperature values on the top copper surface of a single LED system and the comparison with the experimental data (c) the numerical results of mesh independency study.

$$Nu_{approx.} = C\, Re^{a} Pr^{b} = 0.8\, Re^{0.4} Pr^{1/3} \tag{40}$$

In Equation (40), constants C, a, b was predicted about 0.8, 0.4, and 1/3, respectively, for all LED systems in this study. As a result, these Nusselt number correlations had nearly the same properties, but the temperature difference between inlet and outlet surfaces for the multi-LED system was higher than the temperature values obtained for a single LED system, therefore these effects the properties of coolant and also Nusselt number predictions. However, there were no significant changes observed for the Nusselt number predictions under simulated thermal conditions. But, when the temperature variations are large enough, variable properties have to be used to predict Nusselt number.

The calculated junction temperature versus different mass flow rates are demonstrated in Fig. 8c and d. The maximum junction temperature was calculated about 69 °C and 74 °C for single and multi-LED systems for the case of 0.001 kg/s mass flow rate, which was lower than the upper limit of the junction temperature of 150 °C so that LED operated without damage. Another important result

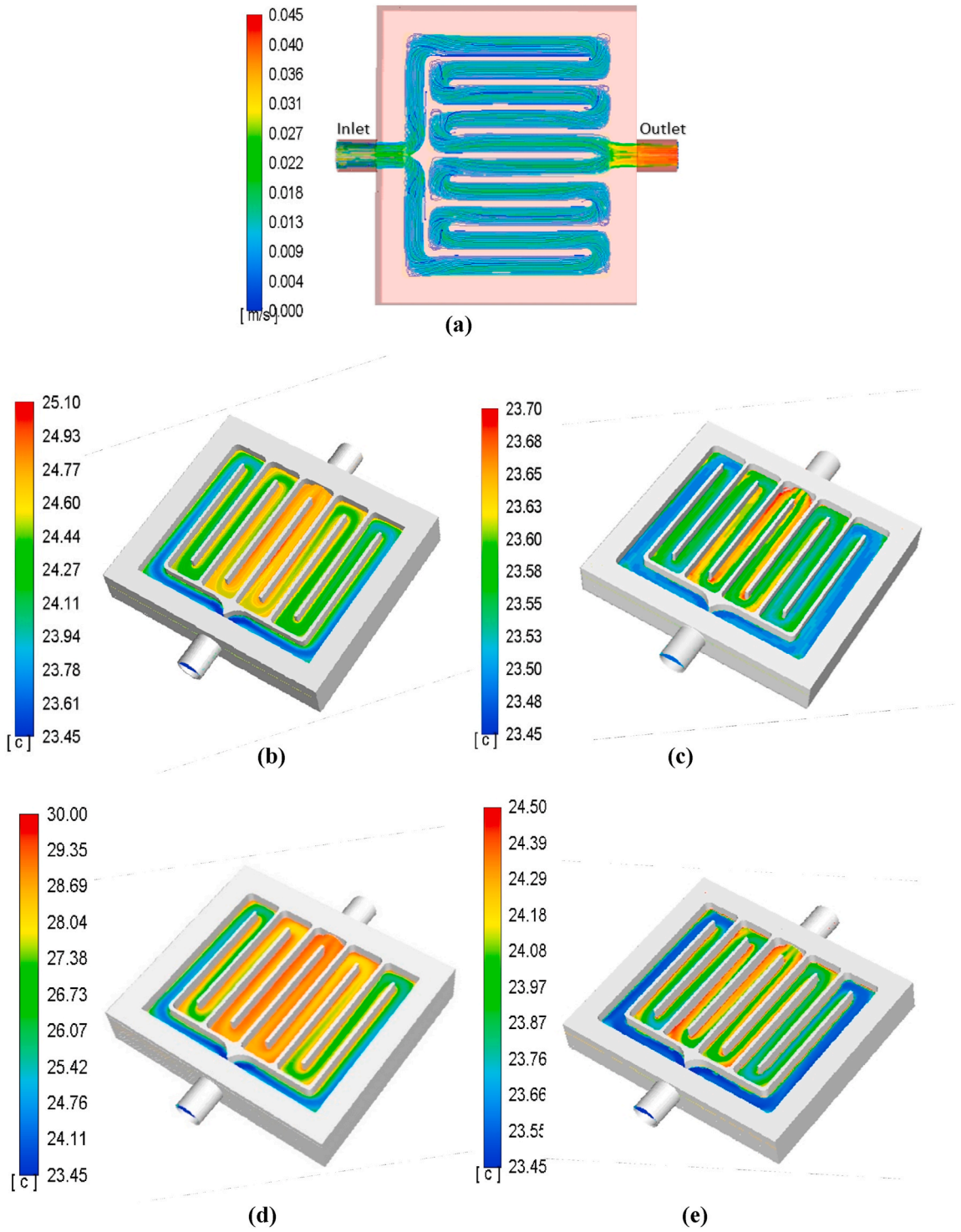


Fig. 6. (a) The calculated velocity (m/s) values of all LED systems for the case of 0.001 kg/s mass flow rate, the calculated temperature (°C) values on the middle section using a single LED: (b) for the case of 0.0005 kg/s and (c) for the case of 0.004 kg/s, the calculated temperature (°C) values on the middle section using multi-LED: (d) for the case of 0.0005 kg/s and (e) for the case of 0.004 kg/s.

was that when using the multi-LED system with a dual-separated cooling channel, the decrease in junction temperature was 3.5 °C and this value was higher than the value obtained for a single LED system, which was calculated about 0.6 °C. On the other hand, the calculated light output with or without using the dual-separated cooling channel was about 563 lm and 510 lm, respectively. This

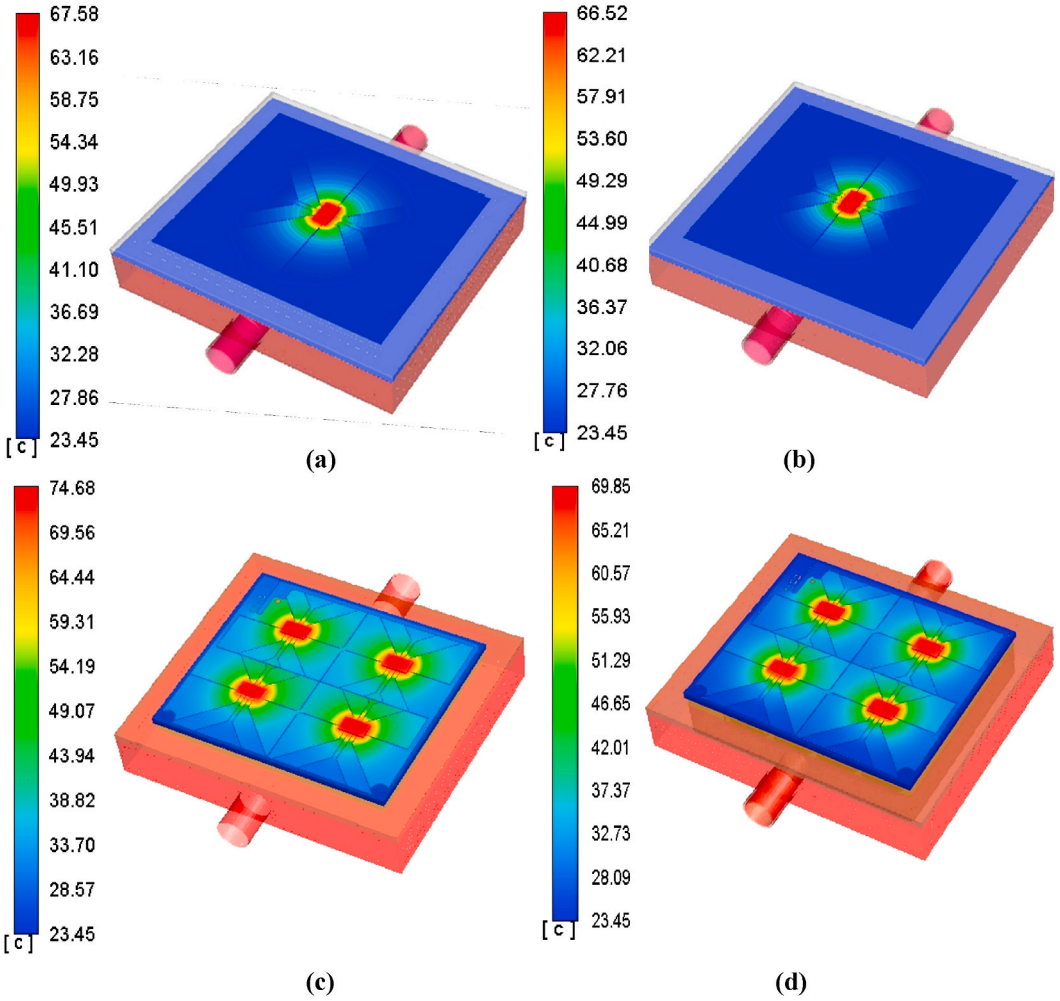


Fig. 7. Calculated temperature (°C) distributions on the top-copper surface of a single LED: (a) for the case of 0.0005 kg/s and (b) for the case of 0.004 kg/s, the calculated temperature (°C) distributions on the top-copper surface of multi-LED: (c) for the case of 0.0005 kg/s mass flow rate and (d) for the case of 0.004 kg/s mass flow rate.

means that the increase in light output with using a dual-separated cooling channel was about 10% for all cases; otherwise, higher junction temperature values lead to a decrease in luminance as well as a reduction in operating efficiency. Not only thermal and hydraulic performance but also lighting characteristics have to assess when to design a cooling system of automotive lighting components, and the foremost important lighting parameter is light output depends on junction temperature, which have a great effect on driver safety.

4. Conclusions

In this paper, the thermal and hydraulic performance analysis of the novel LED cooling block with dual-separated liquid cooling channel were performed for the cooling applications of the single LED and multi-LEDs PCBs utilizing in the automotive lighting system. For this purpose, the LED PCBs and the dual-separated liquid cooling block with real dimensions were designed and manufactured to be employed in the experimental study. A detailed hydraulic analysis in terms of fanning friction factor and the total pressure drop was introduced for evaluating the developing laminar flow in the dual-channel cooling block. A realistic three dimensional CFD model

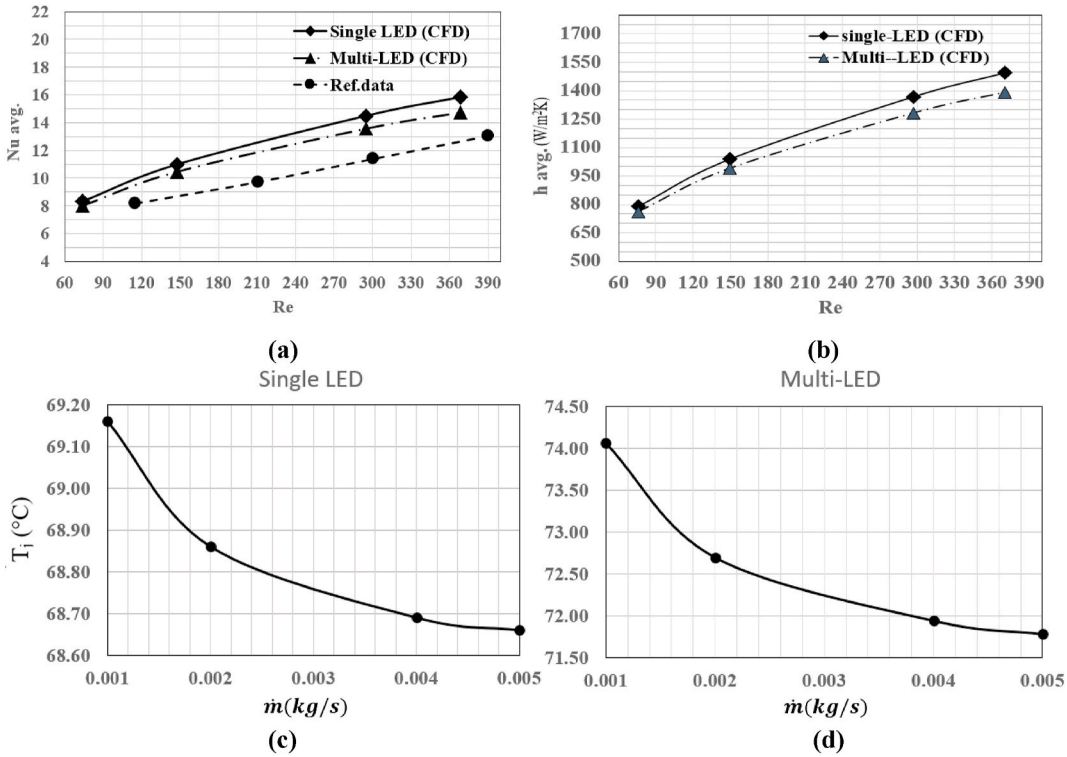


Fig. 8. (a) The comparative results of average Nusselt number versus Reynolds number and comparison to the reference data [31] and (b) the calculated average heat transfer coefficient (W/m^{2}K) depends on mass flow rate, the calculated junction temperature (°C) versus mass flow rate (c) for a single LED and (d) multi-LED systems.

included temperature-dependent properties was realized to get the fluid flow and conjugate heat transfer analysis of the LED PCB cooling system. The model was validated with theoretical analysis and the experimental measurements. It was shown that the numerical results had well compromised with the theoretical and experimental data presented in this study. A detailed numerical and theoretical analysis was performed to obtain a comparative performance evaluation of the cooling block utilizing the different powers of single and multi-LEDs PCBs. With the considerations given above, the conclusions can be stated as follows:

- The dual-separated cooling channel block was suitable for providing an efficient cooling of both single and multi-LED systems used in this study. The decrease in temperature was higher than 50% on the top copper surface contact with a single LED chip, and the junction temperature had been reduced by 36% to ensure desired operating conditions compared to the without cooling condition. The light output quality was also increased about 10% in luminance by using the cooling block.
- Lighting characteristics of automobile head lamps can be improved by using liquid cooling block thus these cooling blocks contribute to the driver visibility and also safety.
- Increasing mass flow rate provided better cooling and controlled on the junction temperature, but it resulted a significant increase in total pressure drop as well as required pumping power. Therefore, optimization must be performed between the thermal performance and the pumping power.
- The calculated average Nusselt number for fully developed laminar flow was a constant value, and however, for developing laminar flow, the computed Nusselt number increased with Reynolds number. The calculated average Nusselt number varied from 8.35 to 15.82 for a single LED system, and this value changed between 8.03 and 14.72 for the multi-LED system in general.
- The increase in temperature of the water was predicted at about 6 °C for the case of 0.0005 kg/s due to high heat transfer from the multi-LED system and this value was calculated about 1.5 °C for the same mass flow rate.
- Two new Nusselt number correlations with temperature-dependent properties were proposed for the separated cooling channel block utilizing a single and multi-LED system. In addition to that, a general (averaged) correlation of Nusselt number was also proposed for the design of similar cooling blocks.

CRediT authorship contribution statement

Gökhan Sevilgen: Methodology, Software, Writing – original draft. **Muhsin Kiliç:** Supervision, Conceptualization, Validation. **Mehmet Aktaş:** Writing – review & editing.

Declaration of competing interest

The authors declare that they have no known competing financial interests or personal relationships that could have appeared to influence the work reported in this paper.

Acknowledgement

The authors wish to thank the Scientific and Technological Research Council of Turkey (TUBITAK) for supporting this research under the project number 5160107- TÜBİTAK 1505.

References

[1] Y. Lai, N. Cordero, F. Barthel, F. Tebbe, J. Kuhn, R. Apfelbeck, D. Würtenberger, Liquid cooling of bright leds for automotive applications, Appl. Therm. Eng. 29 (2009) 1239–1244.
[2] P. Mashkov, B. Gyoch, R. Ivanov, Investigation of Characteristics and Thermal Loading of Led Bulbs for Automotive Headlights, in: Transport Problems, vol. 13, Silesian University of Technology, 2018, pp. 85–95.
[3] Lighting manufacturer, matrix led headlights: redefine adaptive front-lighting with smart high beam technology. https://www.manufacturer.lighting/info/162/ .
[4] H.T. Zwahlen, T. Schnell, Driver-headlamp dimensions, driver characteristics, and vehicle and environmental factors in retroreflective target visibility calculations, Transport. Resear. Record 1692 (1999) 106–118.
[5] R. Elvik, Meta-Analysis of Evaluations of Public Lighting as Accident Countermeasure, vol. 1485, Transportation Research Record, TRB, National Research Council, Washington, D.C., 1995, pp. 112–123.
[6] R.H. Poelma, S. Tarashioon, H.W. van Zeijl, S. Goldbach, J.L.J. Zijl, G.Q. Zhang, Multi-LED package design fabrication and thermal-analysis, J. Semiconduct. 34 (2013).
[7] A. Keppens, H.L. Chen, Z. Chen, Y. Gao, G. Deconinck, P. Hanselaer, Light-Emitting diode junction temperature and power determination from forward current, Light Eng. 19 (2011) 34–44.
[8] A. Rammohan, C. Ramesh Kumar, Performance analysis of cooling system designed for a high power light emitting diode (HPLED) of an automotive headlamp and it's effect on light intensity, Eur. Phys. J. Spec. Top. 228 (2019) 2495–2509.
[9] J.R. Pryde, Development of Effective Thermal Management Strategies for LED Luminaires. A Doctoral Thesis Submitted in Partial Fulfilment of the Requirements for the Award of Doctor of Philosophy of Loughborough University, Wolfson School of Mechanical and Manufacturing Engineering, September 2017.
[10] A. Fan, R. Bonner, S. Sharratt, Y.S. Ju, An innovative passive cooling method for high performance light-emitting diodes, in: 28th Annual IEEE Semiconductor Thermal Measurement and Management Symposium, SEMI-THERM), 2012.
[11] H. Sørensen, Water cooling of high power light emitting diode, in: Proceedings of the 13th IEEE Intersociety Conference on Thermal and Thermomechanical Phenomena in Electronic Systems, ITherm), 2012.
[12] H.T. Chen, X.F. Zhou, Y. Zhang, S. Lin, J.R. Zhou, Y. Fei, Study on the staggered array of an LED system for improved thermal behavior, Appl. Opt. 54 (2015) 6752–6757.
[13] E. Schütt, Thermal Management and Design Optimization for a High Power LED Work Light, Degree Thesis Plastics Technology, 2014.
[14] S.D. Thakre, V.B. Swami, P.T. Malwe, Cooling system of electronic devices using microchannel heat sink, Int. J. Tumor Ther. 4 (2014).
[15] A.F. Al-Neama, N. Kapur, J. Summers, H.M. Thompson, An experimental and numerical investigation of the use of liquid flow in serpentine microchannels for microelectronics cooling, Appl. Therm. Eng. 116 (2017) 709–723.
[16] J. Zhang, Cooling of Electronic System: From Electronic Chips to Data Centers, PhD Dissertation, The State University of New Jersey, Rutgers, 2012, pp. 3–4.
[17] F. Cano-Banda, U.C. Gonzalez-Valle, S. Tarazona-Cardenas, A. Hernandez-Guerrero, Effect of different geometry flow pattern on heat sink performance, in: 12th International Conference on Heat Transfer, Fluid Mechanics and Thermodynamics, 2016.
[18] X. Hao, B. Peng, G. Xie, Y. Chen, Thermal analysis and experimental validation of laminar heat transfer and pressure drop in serpentine channel heat sinks for electronic cooling, J. Electron. Packag. 136 (2014).
[19] R.K. Shah, A.L. London, Laminar Flow Forced Convection in Ducts. Supplement 1 to Advances in Heat Transfer, Academic Press, New York, 1978.
[20] R.K. Shah, A correlation for laminar hydrodynamics entry length solution for circular and noncircular ducts, J. Fluid Eng. 100 (1978) 177–179.
[21] M. Mirmanto, Developing flow pressure drop and friction factor of water in copper microchannels, J. Mech. Eng. Autom. 3 (2013) 641–649.
[22] S. Maharudrayya, S. Jayanti, A.P. Deshpande, Pressure losses in laminar flow through serpentine channels in fuel cell stacks, J. Power Sources 138 (2014) 1–13.
[23] I.E. Idelchik, Handbook of Hydraulic Resistance, Hemisphere Publishing, New York, 1986.
[24] R.J. Philips, Forced-convection Liquid-Cooled Microchannel Heat Sinks, Master Thesis. Massachusetts Institute of Technology, Cambridge MA, 1987.
[25] Ansys Fluent 12.0 Theory Guide. Release 12.0 © ANSYS. Inc, 2009-01-23.
[26] M. Kılıç, M. Aktaş, G. Sevilgen, Ş. Kaya, The numerical and experimental investigation of the thermal performance of led circuit boards used in automotive lighting systems, in: 9 Th International Automotive Technologies Congress, 2018.
[27] G. Sevilgen, M. Kilic, Transient numerical analysis of airflow and heat transfer in a vehicle cabin during heating period, Int. J. Veh. Des. 52 (2010) 144–159.
[28] M. Kilic, G. Sevilgen, Evaluation of heat transfer characteristics in an automobile cabin with a virtual manikin during heating period, Numer. Heat Tran. Part A-Applications 56 (2009) 515–539.
[29] M. Mutlu, G. Sevilgen, M. Kiliç, Evaluation of windshield defogging process in an automobile, Int. J. Veh. Des. 71 (2016) 103–121.
[30] R.J. Moffat, Describing the uncertainties in experimental results, Exp. Therm. Fluid Sci. 1 (1988) 3–17.
[31] P.S. Lee, S.V. Garimella, Thermally developing flow and heat transfer in rectangular microchannels of different aspect ratios, Int. J. Heat Mass Tran. 49 (2006) 3060–3067.
[32] A.A. Imrana, N.S. Mahmouda, H.M. Jaffal, Numerical and experimental investigation of heat transfer in liquid cooling serpentine mini-channel heat sink with different new configuration models, Therm. Sci. Eng. Progr. 6 (2018) 128–139.
[33] M. Kılıç, M. Aktaş, G. Sevilgen, Thermal assessment of laminar flow liquid cooling blocks for LED circuit boards used in automotive headlight assemblies, Energies 13 (2020).
[34] M. Kılıç, A. Yiğit, Isı Transferi, Tablo B.7. Doymuş Suyun Termofiziksel Özelikleri, pp.476.

[35] M. Kılıç, M. Aktaş, G. Sevilgen, Liquid cooling performance of the single and multi led circuit boards used in automotive lighting systems, in: 2019 4th International Conference on Smart and Sustainable Technologies, SpliTech, 2019, https://doi.org/10.23919/SpliTech.2019.8783136. IEEE Xplore, Article Number 8783136, 2019.
[36] M. Aktaş, G. Sevilgen, M. Kılıç, Design and Performance Evaluation of Liquid Cooling Blocks with Fins for Led Circuit Boards Used in Automotive Lighting Systems, in: 22nd Congress on Thermal Science and Technology (ULIBTK'19), 11–14 September, Kocaeli, TURKEY, 2019.
[37] A. Muhammad, D. Selvakumar, A. Iranzo, Q. Sultan, J. Wu, Comparison of pressure drop and heat transfer performance for liquid metal cooled mini-channel with different coolants and heat sink materials, J. Therm. Anal. Calorim. 141 (2020) 289–300.
[38] M.U. Sajid, H.F. Ali, A. Sufyan, D. Rashid, S.U. Zahid, W.U. Rehman, Experimental investigation of TiO_2–water nanofluid flow and heat transfer inside wavy mini-channel heat sinks, J. Therm. Anal. Calorim. 137 (2019) 1279–1294.
[39] J.P. Sharma, A. Sharma, R.D. Jilte, R. Kumar, M.H. Ahmadi, A study on thermohydraulic characteristics of fluid flow through microchannels, J. Therm. Anal. Calorim. 140 (2020) 1–32.
[40] G. Sevilgen, G. Sayaral, M. Kilic, H. Bayram, Investigation of thermal sensation in a railway vehicle during cooling period, Transport. Res. Rec. 2674 (2020) 461–474.
[41] R. Abbasgholi Rezaei, S. Jafarmadar, S. Khorasani, Presentation of frictional behavior of micro helical tubes with various geometries and related empirical correlation; an experimental study, Int. J. Therm. Sci. 140 (2019) 377–387.
[42] M.W. Tian, S. Khorasani, H. Moria, S. Pourhedayat, H. Sadighi Dizaji, Profit and efficiency boost of triangular vortex-generators by novel techniques, Int. J. Heat Mass Tran. 156 (2020) 119842.
[43] N. Sinaga, S. Khorasani, K. Sooppy Nisar, A. Kaood, Second law efficiency analysis of air injection into inner tube of double tube heat exchanger, Alexandria Eng. J. 60 (2021) 1465–1476.

Nomenclature

A_{ch}: The cross sectional area ıf the cooling channel [m^2]
A_s: Total heat transfer surface area [m^2]
A_{in}: Cross sectional area of inlet for the contraction or extraction region [m^2]
A_{out}: Cross sectional area of the outlet for the contraction or extraction region [m^2]
c: Fitting factor
c_p: Specific heat of fluid.[J/kgK]
C_r: Curvature ratio
D_h: Hydraulic diameter [m]
f: Fanning friction factor
f_{app}: Apparent friction factor
f_{frd}: Fanning friction factor for fully developed flow
h_{avg}: Average heat transfer coefficient [W/ m^2K]
H_c: Height of the channel. [m]
I: Current [A]
k_f: Thermal conductivity of fluid [W/ mK]
k_s: Thermal conductivity of solid [W/ mK]
$K(\infty)$: Incremental pressure drop for fully developed flow region
$K_{b,j}$: Bending loss coefficient
K_c: Contraction loss coefficient
K_e: Extraction loss coefficient
L: Total length of the channel [m]
L_h: Hydrodynamic entrance length [m]
L^+: Dimensionless channel length
$\dot{m}$: Total mass flow rate [kg/s]
$\dot{V}_p$: Flow rate of the recirculation pump [l/min]
n: Number of returns in the cooling channel
Nu: Nusselt number
P_{LED}: Power of LED [W]
Pr: Prandtl numer
$\Delta P_{bj,90^\circ}$: Pressure drop due to 90° bending for j th bending [Pa]
$\Delta P_{bi,180^\circ}$: Pressure drop due to 180° returns for i th return [Pa]
ΔP_c: Pressure drop due to sudden contraction [Pa]
ΔP_e: Pressure drop due to sudden extraction [Pa]
ΔP_f: Pressure drop due to friction [Pa]
ΔP_{total}: Total pressure drop [Pa]
q_{loss}: Heat loss for the lighting function [W]
$\dot{Q}_b$: Total heat transfer rate occurred in the cooling block [W]
Re: Reynolds number
$R_{th,Jp}$: Thermal resistance of the junction point [°C/W]
S: Source term includes heat generation for LED part [W/m^3]
T: Temperature [°C, K]
T_{in}: Temperature of the fluid before entering the cooling block [°C]
T_{out}: Temperature of the fluid after leaving the cooling block [°C]
T_j: LED junction temperature [°C]
T_{max}: Maximum temperature [°C]
ΔT_{lm}: Logarithmic temperature difference [°C]
U_{ch}: Average flow velocity in the channel [m/s]
x, y, z: Coordinates [m]
V: Voltage [V]
$\vec{V}$: Velocity vector [m/s]
W_c: Width of the channel [m]
W_t: Thickness of the channel [m]

Greek Symbols

α: Aspect ratio
β: Ratio of the height of the channel height to its width

ρ: Density [kg/m^3]
ξ: Bending loss coefficient
μ: Dynamic viscosity of fluid [Pa.s]

Subscripts

Avg: Average
b: Block
c: Contraction
e: Extraction
f: Fluid
fd: Fully develop
in: Inlet
lm: Lumen
max: Maximum
out: Outlet